

Shock Induced Electrical Activation in Structurally Detailed Models of Pig Left-Ventricular Tissue

Mark L. Trew¹, Jesse L. Ashton¹, Bryan J. Caldwell¹, and Bruce H. Smail^{1,2}

Abstract—Detailed models of sample specific structures in pig left-ventricular tissue have been constructed. These models include epicardial and endocardial surfaces, fiber and sheet orientations, vessels and cleavage planes with significant dimensions. This work shows that it is possible to extract from 3D tissue images reduced dimension descriptions of cleavage planes in the heart wall. These descriptions are used to analyze the response of tissue to electrical shocks of varying strengths. The presence of explicit discontinuities in the heart significantly reduces the time required for transmural activation and provides a basis for understanding successful defibrillation.

I. INTRODUCTION

PREDICTING patterns of cardiac activation within the heart wall following defibrillation-strength shock treatment is potentially of great value for understanding and improving the efficiency of cardioversion. There is a growing emphasis on investigating the onset and control of abnormal cardiac rhythm using computer models based on detailed structural geometry of whole or part ventricles [1,2,3]. In this paper we report on the development of a detailed wedge model of tissue structures in the pig left-ventricle (LV). The model is used to analyze activation resulting from the transmural shock stimulation of quiescent tissue.

Ventricular myocytes are arranged in discrete laminar layers separated by collagenous septae [4], or cleavage planes [5]. The organization of myocytes significantly affects cardiac electrical activity [6] and shock response [7]. It is argued that formation of virtual electrodes (VEs) at sites of structural discontinuities or heterogeneities within the LV wall is necessary to explain successful cardioversion [5,7,8].

Mechanisms that underlie this distributed VE formation are well understood [9]. Small scale variations in fiber orientation, discontinuities associated with cleavage planes and blood vessels cause current driven by externally applied fields to spatially vary its distribution between intra- and extracellular spaces resulting in positive and negative membrane polarizations. To account for these outcomes in computer models, detailed tissue structural information must be included.

Previous work analyzing relationships between shock

response and tissue structure was restricted to small rat heart samples [3,5]. That analysis provided important insights into intramural tissue response to electric shock. However, there remained outstanding questions regarding the nature of response in significantly larger tissue volumes. Experimental studies have been conducted using wedge preparations from larger hearts such as pig [7]. Whereas it is feasible to extract cleavage plane descriptions manually for small tissue samples [5], this is not the case for large tissue samples. However, the new methods described in this paper have now enabled the automatic reduction of cleavage plane discontinuities to collections of 2D finite elements. A unique feature of the modeling approach presented in this paper is the layers of structural information that can be added or removed to test hypotheses regarding structural scales influencing tissue response to shock stimulation.

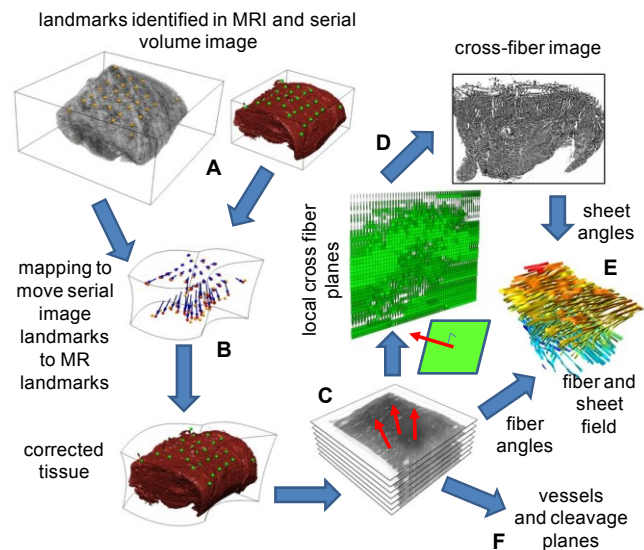


Fig. 1. Structural model creation pipeline. **A:** Tissue imaged using MR and extended volume serial imaging. **B:** Serial images corrected for distortions by matching landmarks with MR images. **C:** Fiber orientations extracted from image planes parallel to epicardium. **D:** Windows orthogonal to local fiber orientation are used to construct cross-fiber images that sheet angles are directly measured from. **E:** Fiber and sheet fields combined into a single description. **F:** Corrected image stack C is processed separately to segment vessels and extract cleavage planes.

II. METHODS

A. Tissue Structural Model

Tissue from the LV free wall of pig hearts was fixed and imaged using a 1.5T MR scanner at $0.312 \times 0.312 \times 0.3 \text{ mm}^3$ resolution then wax-embedded and serially imaged through the tissue volume [10] at $8.33 \mu\text{m}$ pixel in-plane resolution

This work was supported by the Health Research Council of New Zealand.

¹Auckland Bioengineering Institute, University of Auckland, New Zealand.

²Department of Physiology, University of Auckland, New Zealand.

Corresponding author: M.L. Trew (+64-9-373-7599x85114; fax: +64-9-367-7157; e-mail: m.trew@auckland.ac.nz).

and either 50 μm or 16.7 μm inter-plane resolution (Fig. 1A). Landmarks visible in both modalities were identified and used for correcting tissue processing distortions (Fig. 1B) [11]. The corrected images were then resliced/resampled as required.

Fiber orientations throughout the tissue wall were determined using image intensity gradients (Fig. 1C). Using the fiber vectors, $480 \times 480 \mu\text{m}^2$ windows orthogonal to each vector were defined and the 3D tissue structure was mapped onto each window producing a stack of local cross-fiber images (Fig. 1D shows sample windows and a corresponding image). Each window is a tissue structure view down the fiber vector. Sheet and sheet normal directions were directly measured using the same method as the fibers. The fiber and sheet angles were combined into a single field description (Fig. 1E). Structural features such as vessels and explicit cleavage planes were identified or computed from the corrected serial volume image (Fig. 1F).

B. Computing Cleavage Planes

The tissue images were processed using local normalizations and thresholding [11] into 1 bit image masks of non-myocardial cleavage planes (Fig. 2A) at 10 μm voxel resolution. These formed the basis of explicit cleavage plane descriptions for electrical activation modeling. Subsampling the images to match a typical 50-150 μm computer modeling mesh resolution caused loss of cleavage plane topology and connectivity and an over-expression of plane volume. Previous success projecting reduced dimension descriptions of cleavage planes [5,12], i.e. 2D descriptions in 3D space, onto computational meshes motivated the development of a new algorithm for the effective 3D skeletonization of the cleavage plane mask, summarized in Fig. 2.

The method divided the mask image into sub-images of predetermined dimension, which dictated the scale of cleavage planes that were expressed. A sub-image dimension of 0.25 mm (25^3 voxels) was chosen in this work. Structural features within the sub-image were ignored and a 2D skeletonization (morphological operation) was performed on each face of the sub-image (Fig. 2C). This skeletonization was divided into connected groups of pixels of significant length and the total number of pixels was reduced by discarding the remainder. For each group (cleavage plane) of retained pixels, a template of $12 \times 2\text{D}$ bilinear finite elements (FEs) provided possible options for a cleavage plane description within the sub-image. The node common to all 12 FEs was chosen to be the 3D center-of-mass (COM) of all pixels in that group. Nodal locations on faces were given by the 2D COM for that face and locations on edges were given by the 1D COM for that edge. Nodes and FEs were not constructed for COMs that did not exist. In this manner 2D FEs representing a cleavage plane within a sub-image were rapidly constructed. The method ensured that FEs were consistent between sub-images. The reduced dimension 2D FE descriptions of the laminar structures were projected onto computational meshes as described

previously [5,12].

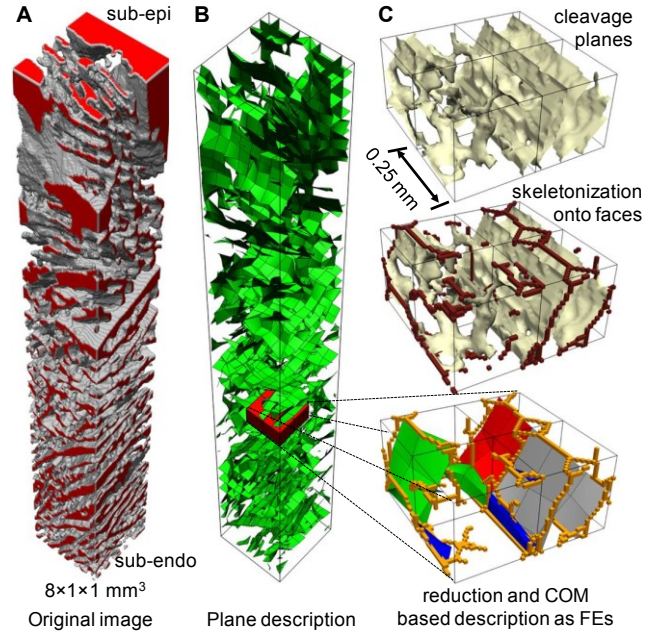


Fig. 2. Extracting finite element descriptions of cleavage planes. **A:** Original image stack with cleavage planes highlighted. **B:** Cleavage planes expressed as 2D finite elements. **C:** Converting volumes to planes: laminar structure is skeletonized on faces of 0.25^3mm^3 sub-images of the 3D image; skeletonization is reduced and group center-of-mass locations in the volume ($\times 1$), on faces ($\times 6$) and on edges ($\times 12$) are used to define nodal locations of a 12 element template.

C. Cardiac Activation Modeling

Electrical behavior was represented by the bi-domain model (1), with intracellular (myocardial) and extracellular domains communicating through the membrane ionic current, I_{ion} . The dependent variables are the transmembrane potential, V_m , and the extracellular potential, ϕ_e .

$$A_m C_m \frac{\partial V_m}{\partial t} - \nabla \cdot (\boldsymbol{\sigma}_i \nabla V_m) = \nabla \cdot (\boldsymbol{\sigma}_i \nabla \phi_e) - A_m I_{\text{ion}} \quad (1)$$

$$\nabla \cdot ((\boldsymbol{\sigma}_e + \boldsymbol{\sigma}_i) \nabla \phi_e) = -\nabla \cdot (\boldsymbol{\sigma}_i \nabla V_m) - i_e$$

Here A_m is the surface to volume ratio of the representative cell membrane between the domains, C_m is the specific capacitance of the membrane, $\boldsymbol{\sigma}_i$ and $\boldsymbol{\sigma}_e$ are the intra- and extra-cellular conductivity tensors and i_e is a current injection per unit volume into the extracellular space.

Assuming isolated tissue, these equations are subject to the no-flux current boundary conditions given in (2).

$$\nabla(V_m + \phi_e) \cdot (\boldsymbol{\sigma}_i \mathbf{n}) = 0 \quad \text{on } \Gamma_o \text{ and } \Gamma_c \quad (2)$$

$$\nabla(\phi_e) \cdot (\boldsymbol{\sigma}_e \mathbf{n}) = 0 \quad \text{on } \Gamma_o$$

Γ_o are the exterior boundaries and Γ_c are the internal boundaries in the intracellular domain, i.e. cleavage planes (e.g. Fig. 2B).

The equations were discretized using a finite volume method [12]. This method is ideally suited for representing planar discontinuities. Given the limited dimensions of the tissue model, it was unrealistic to impose a local ground for the extracellular potential. The pure Neumann problem was

modeled in the elliptic extracellular potential update of (1) with the mean extracellular potential constrained to zero [13]. An advanced multilevel solver strategy [13] was employed to solve this system.

Membrane currents were modeled with a defibrillation-modified LRd model [14,15]. Additional modifications were implemented to increase the robustness of the equations by capturing the critical points of equations with limits tending to 0/0 and ensuring that no equation denominators tended toward 0. The membrane model was written using the CellML markup language (www.cellml.org). In many models these modifications are not necessary. However, the application of a shock across tissue with explicit discontinuities more closely spaced than the tissue space constant results in almost linear variations in V_m during the shock. Together with a relatively fine computational mesh this increases the likelihood of equation evaluations where either the denominator or both numerator and denominator tend to zero.

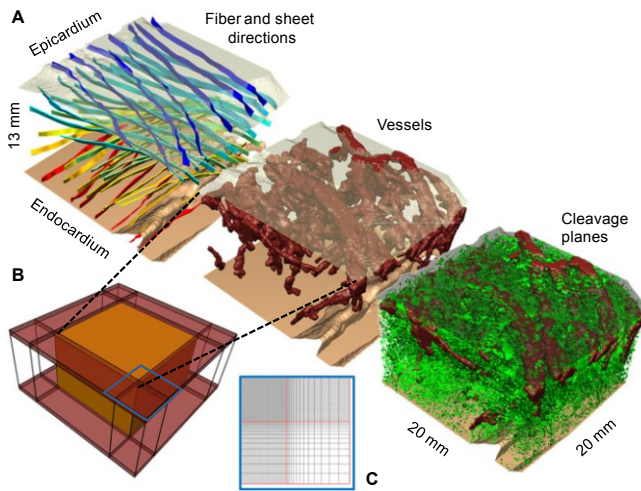


Fig. 3. Tissue model with layers of structural complexity that can be combined. **A:** Models with specified fiber and sheet directions, explicit vessel discontinuities and explicit laminar discontinuities. **B:** 5 mm padding elements surrounding tissue model and 1 mm blood layers on top and bottom. **C:** Graded mesh detail in the padded region.

D. Numerical Tissue Model

The layers of structural detail and the tissue dimensions are shown in Fig. 3. The computational mesh was discretized to 100 μm in all directions, giving approximately 8.5 million solution points. Tissue electrical conductivity parameters were determined by enumerating the intracellular conductivity space in simplified models and matching known experimental conductivity and conduction velocities in pig cardiac tissue [16,17]. The intra- and extracellular conductivity sets best matching observations were: $\sigma_i=(0.35,0.04,0.01)$ mS/mm and $\sigma_e=(0.35,0.31,0.14)$ mS/mm. The models contained three types of domain components: myocardium, extra-epi- and extra-endocardial blood and vessels. The electrical conductivities for blood were based on a typical isotropic literature value of 0.8 mS/mm. Vessel conductivity was reduced to 0.78 mS/mm to

account for the possible influences of a fibrous sheath. Shock stimulations were delivered by plate electrodes located below and above the epicardial and endocardial blood layers. Extracellular current shocks of varying strengths, shapes and durations were considered.

III. RESULTS

A detailed model of the structure of the pig left ventricle heart wall (5.2 cm^3) has been constructed (Fig. 3). This model includes features of the epicardium and endocardium, fiber and sheet orientations, vessels and explicit cleavage planes. The cleavage planes are represented by 792000 2D finite elements. Boundary effects were mitigated by adding 5 mm padding to the wedge in all lateral directions and 1 mm of blood below and above the wedge (Fig. 3B). The padding mesh was graded (Fig. 3C).

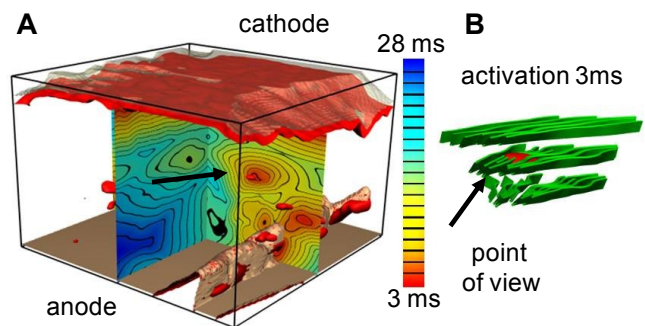


Fig. 4. **A:** Activation times following a 3 ms monophasic shock applied to continuous tissue model with fiber and sheet descriptions and anisotropic electrical conductivities. **B:** Intramural virtual electrode and the local fiber and sheet orientations.

The response of a continuous wedge model to a 3 ms monophasic shock with the cathode on the epicardium and the anode on the endocardium is shown in Fig. 4A. The red isosurfaces denote 3 ms activation time while the contoured planes denote the entire activation sequence. The tissue block is fully activated 28 ms after the shock onset. There are intramural sites where early activation occurs. These relate to rapid local variations in fiber and sheet orientation (Fig. 4B). Early activation also occurs at sites on the anodal side of the endocardial features. In general activation sweeps down from the epicardium, coalesces with intramural virtual cathodes and activates toward the endocardium.

The responses to the same shock protocol for tissue with different levels of explicit discontinuities are shown in Fig. 5. A large number of intramural virtual cathodes formed on the anodal (endocardial) side of the cleavage discontinuities (Fig. 5A,B) and the vessel discontinuities (Fig. 5B). These coalesced, resulting in the tissue block being activated in less than 15 ms (however, 95% of the tissue was activated within 8.5 ms). The presence of both types of discontinuities (Fig. 5B) resulted in greater numbers of virtual cathodes compared to cleavage planes only (Fig. 5A), particularly in the sub-epi and midwall regions.

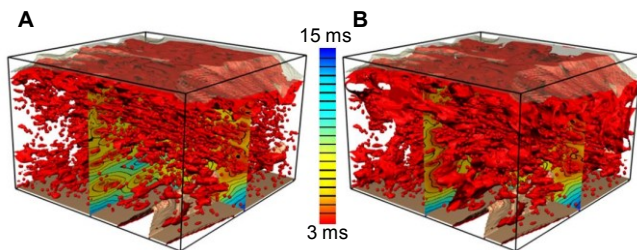


Fig. 5. Shock solutions in discontinuous tissue. **A:** Model with explicit cleavage planes only. **B:** Model with explicit cleavage planes and vessels.

Fig. 6 summarizes the times required to activate 95% (T^{95}) of the tissue volume for various structures, stimulus forms and strengths. Shorter duration 3 ms monophasic shocks rapidly activate the tissue for shock strengths > 5 V/cm but for shocks stronger than approximately 20 V/cm there is minimal additional decrease in T^{95} . For the longer monophasic shock (6 ms) there is an initial decrease in T^{95} as the shock strength increases, however, for stronger shocks (e.g. 32 V/cm) T^{95} increases again. For both duration shocks, the continuous model reached T^{95} later than the discontinuous model, particularly for a 3ms duration shock. The inclusion of vessel discontinuities as well as the explicit cleavage planes reduces T^{95} in the case of both shock durations. Biphasic and reversed polarity shocks also result in a reduced T^{95} compared to the monophasic case.

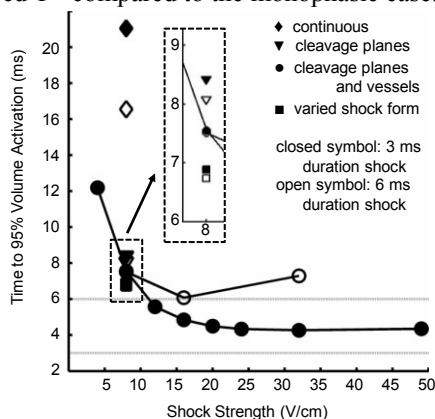


Fig. 6. Time required to activate 95% of quiescent model tissue as a function of potential gradient at shock termination. The varied shock forms are 3ms monophasic reversed polarity and 6 ms biphasic (3+3 ms). Detail for 8 V/cm shocks is shown in the inset.

IV. DISCUSSION

This paper presents a powerful model for investigating the electric shock response of cardiac tissue and for testing various forms of therapy. The tissue volume is large enough to support reentry and the response of active tissue to electric shocks will be a focus of future study.

The observation that with increasing shock strengths T^{95} decreases to remain approximately constant at 4 ms for the shorter duration shock but grows for the longer duration shock mimics observations made in simulations using rat heart tissue. This reflects the increasing influence of regions of hyperpolarisation on the cathode side of discontinuities as the shock strength and duration increase. The interplay between positive and negative polarization can also be

invoked to explain why biphasic shocks result in a lower T^{95} , while the physical distribution of discontinuities in the sub-epi and midwall regions explains the effects due to reversed shock polarity.

A consequence of the choice of sub-image dimension is that the dense, smaller cleavage planes, particularly in the sub-endo region are under-represented (Fig. 2A,B). However, due to their dimension, the effect may be more significant at the level of propagation from a point stimulus than as a source of virtual electrodes. To account for the possible effects of discarding smaller planes on post-shock propagation the anisotropic conductivity was used in the discontinuous models, based on the sheet orientation field.

REFERENCES

- [1] A. P. Benson, *et al.*, "The canine virtual ventricular wall: a platform for dissecting pharmacological effects on propagation and arrhythmogenesis," *Prog Bio Mol Bio*, vol. 96, pp. 187-208, 2008.
- [2] F. Vadakkumpadan, *et al.*, "Image-based models of cardiac structure with applications in arrhythmia and defibrillation studies," *J Electrocard*, vol. 42, pp. 157.e1-157.e10, 2009
- [3] D.A. Hooks, *et al.*, "Do intramural virtual electrodes facilitate successful defibrillation? Model-based analysis of experimental evidence," *J Cardiovas Electrophysiol*, vol. 17, no. 3, pp. 305-311, 2006.
- [4] I.J. LeGrice, *et al.*, "Laminar structure of the heart: ventricular myocyte arrangement and connective tissue architecture in the dog," *Am J Physiol*, vol. 269, pp. H571-H582, 1995.
- [5] D.A. Hooks, *et al.*, "Cardiac microstructure: implications for electrical propagation and defibrillation in the heart," *Circ Res*, vol. 91, no. 4, pp. 331-338, 2002.
- [6] M.S. Spach and P.C. Dolber, "Relating extracellular potentials and their derivatives to anisotropic propagation at a microscopic level in human cardiac muscle," *Circ Res*, vol. 58, pp. 356-371, 1986.
- [7] O.F. Sharifov and V.G. Fast, "Optical mapping of transmural activation induced by electrical shocks in isolated left ventricular wall wedge preparations," *J Cardiovas Electrophysiol*, vol. 14, no. 11, pp. 1215-1222, 2003.
- [8] N. Mazeh and B.J. Roth, "A Mechanism for the Upper Limit of Vulnerability," *Heart Rhythm*, vol. 6, no. 3, pp. 361-367, 2009.
- [9] B.J. Roth, "How to explain why 'unequal anisotropy ratios' is important using pictures but no mathematics," *Proc 28th IEEE EMBS*, pp. 580-583, 2006.
- [10] D.A. Gerneke, *et al.*, "Surface imaging microscopy using an ultramiller for large volume 3D reconstruction of wax- and resin-embedded tissues," *Micros Res Tech*, vol. 70, no. 10, pp 886-894, 2007.
- [11] M.L. Trew, *et al.*, "Experiment-specific models of ventricular electrical activation: construction and application," *Proc 30th IEEE EMBS*, pp. 137-140, 2008.
- [12] M.L. Trew, I.J. LeGrice, B.H. Smaill and A.J. Pullan, "A finite volume method for modeling discontinuous electrical activation in cardiac tissue," *Ann Biomed Eng*, vol. 33, no. 5, pp. 590-602, 2005.
- [13] T.A. Austin, M.L. Trew and A.J. Pullan, "Solving the cardiac bidomain equations for discontinuous conductivities," *IEEE Trans Biomed Eng*, vol. 53, no. 7, pp. 1265-1272, 2006.
- [14] G.M. Faber and Y. Rudy, "Action potential and contractility changes in [Na⁺]_i overloaded cardiac myocytes: a simulation study," *Biophys J*, vol. 78, pp. 2392-2404, 2000.
- [15] T. Ashihara and N.A. Tryanova, "Asymmetry in membrane responses to electric shocks: insights from bidomain simulations," *Biophys J*, vol. 87, pp. 2271-2282, 2004.
- [16] D.A. Hooks, *et al.*, "Laminar arrangement of ventricular myocytes influences electrical behavior of the heart," *Circ Res*, vol. 101, pp. e103-e112, 2007.
- [17] B.J. Caldwell, *et al.*, "Three distinct directions of intramural activation reveal non-uniform side-to-side electrical coupling of ventricular myocytes," *Circulation Arrhy Elect*, in press, 2009.